10-21-2003

$CoGe_{1.5}Se_{1.5}$: Structural and Transport Properties Characterization

Randolph Ertenberg
University of South Florida

$CoGe_{1.5}Se_{1.5}$: Structural and Transport Properties Characterization

by

Randolph Ertenberg

A thesis submitted in partial fulfillment
of the requirements for the degree of
Master of Science
Department of Physics
College of Arts and Sciences
University of South Florida

Major Professor: George S. Nolas, Ph.D.
Robert Chang, Ph.D.
Pritish Mukherjee, Ph.D.

Date of Approval:
October 21, 2003

Keywords: Thermoelectric, Semiconductor, Skutterudite, Material, Physics

Acknowledgements

I would like to thank Dr. Jihui Yang for carrying out low temperature measurements.

Table of Contents

List of Tables

List of Figures

$CoGe_{1.5}Se_{1.5}$: Structural and Transport Properties Characterization

Randolph Ertenberg

ABSTRACT

Skutterudites have been of great interest for thermoelectric applications over the last ten years. Scientific interest has focused on the unique transport properties Skutterudites possess due to the unique crystal structure. Technical interest has grown since it was discovered that some compounds rival the current best thermoelectric materials. To further the understanding of this material system, and optimize its thermoelectric properties, the synthesis and characterization of polycrystalline *n*- and *p*-type $CoGe_{1.5}Se_{1.5}$ was undertaken. Structural, morphological, chemical, electrical, thermal and magnetic properties were studied. These data are compared to those of the binary Skutterudite $CoSb_3$. The results of this study show a very sensitive dependence of the physical properties on stoichiometry. While the thermoelectric figure of merit is low in these materials, it is apparent that optimization via doping and "void filling" will lead to improved thermoelectric properties.

Chapter One: Thermoelectrics

1.1 Overview

The long struggle to achieve high efficiency refrigeration or power generation with thermoelectrics began in the early 1800's when Thomas Seebeck and Jean Peltier explored the relationships between temperature and electricity in materials. In 1821, Seebeck [1] discovered that a junction between two dissimilar materials, A and B, exposed to a temperature gradient formed an electric potential. (Figure 1-1)

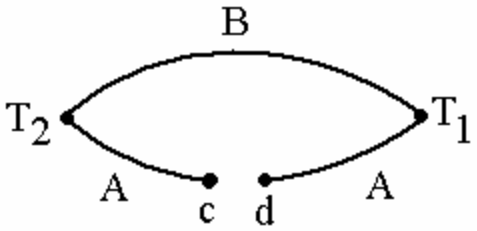

Figure 1-1. **Seebeck Effect Illustrated.** Junctions between two dissimilar materials, A and B are exposed to a temperature difference between T_1 and T_2, and a voltage forms between c and d.

Later, in 1834, Peltier [1] discovered that when a current was run through a junction of two dissimilar materials, such as bismuth and antimony, heating or cooling occurred at the junction. (Figure 1-2) This process was reversible for both heating and for cooling.

These properties, called the Seebeck and Peltier effect respectively, allow the creation of a temperature gradient from a voltage difference, or a voltage difference from

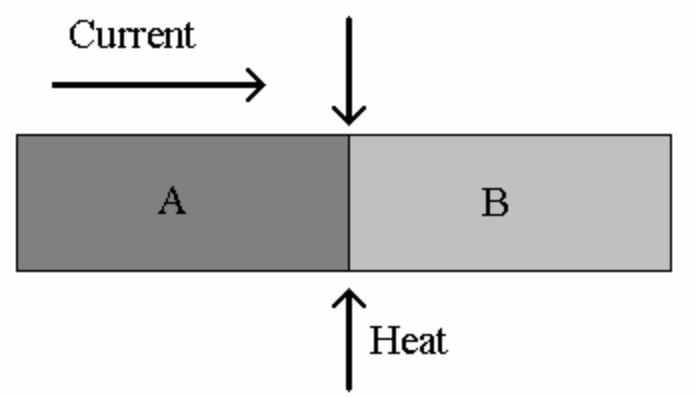

Figure 1-2. **Peltier Effect Illustrated.** The current flows through the junction between the two materials, A and B, causing heat to be absorbed, or cooling. If the current is reversed, heat will be released. Both processes are reversible.

a temperature gradient. Using fundamental thermodynamic arguments, W. Thomson showed the close relationship between the Seebeck and Peltier effects in 1857 [1].

With the exception of Altenkirch's derivation of thermoelectric efficiency in 1911 [2], progress in the field was negligible after the basic thermodynamic effects had been thoroughly described and understood. In the early twentieth century, the microscopic understanding of electronic interactions within crystals was developed. This work led to the materials currently employed for solid-state refrigeration and power generation, namely Bi_2Te_3 alloys and Si-Ge alloys. Bi_2Te_3 alloys have small band gaps and are typically used for refrigeration applications while Si-Ge alloys are optimized for high temperature applications from approximately 600K to 1300K, and have band gaps of about 1 eV.

During the last forty years, small compositional changes have resulted in incremental improvements in the thermoelectric properties of these alloys. However, these materials have changed very little since their discovery more than 40 years ago

while they have not yet been surpassed. It is believed that materials with far better properties can be made, vastly improving the efficiency of thermoelectric devices. One current candidate for this effort are compounds with the Skutterudite crystal structure. This class of materials drew interest for thermoelectric applications when it was realized that it had many of the properties that are desirable for high figures of merit, such as large carrier mobilities and a large unit cell with heavy atomic masses [3]. A most interesting structural aspect of these materials is the presence of voids in the structure that can be interstitially "filled". As will be described later, this significantly lowers the thermal conductivity, an important factor for good thermoelectrics. This unique property makes Skutterudites a material of great interest. In this thesis I will report on a new variant of this structure, $CoGe_{1.5}Se_{1.5}$. Properties important for understanding the physics of these novel materials as well as the potential development for thermoelectric applications, such as structural, morphological, chemical, electrical, thermal and magnetic characteristics, have been investigated. This material shows strong dependence on stoichiometry in that slight variations completely alter the transport properties.

1.2 Introduction to Thermoelectric Materials

A fundamental physical property that is key to the evaluation of thermoelectrics is the Seebeck effect. Its magnitude is given by the Seebeck coefficient, *S*, defined as

$$S = \frac{V}{\Delta T} \qquad (1)$$

where V is the open circuit voltage and ΔT is the difference in temperature. This states that a voltage difference applied to a junction of two dissimilar materials creates a temperature gradient. Conversely, a temperature gradient across a thermoelectric material generates a voltage difference. In general, when the charge carriers are electrons, S is negative, and S is positive for holes.

An overall measure of the thermoelectric potency of a given material is the dimensionless thermoelectric figure of merit, ZT [2], defined as

$$ZT = \frac{S^2 s}{k_e + k_L} T, \qquad (2)$$

where T is the temperature, S is the Seebeck coefficient, s is the electrical conductivity, k_e is the electronic component of the thermal conductivity and k_L is the lattice contribution. Thus the best thermoelectric materials will possess good electrical properties together with a low thermal conductivity. The current best thermoelectrics have $ZT \sim 1$ in the temperature range of interest. This value has been a practical upper limit for more than 30 years, yet no theoretical reason exists for why it cannot be larger [2].

As shown from equation (2), the main characteristics for a good thermoelectric material are high electrical conductivity, high Seebeck coefficient, and low thermal conductivity. What are the fundamental material properties that govern these physical properties and how can they be maximized? To begin to answer these questions, it is useful to think in terms of ideal materials. High Seebeck coefficients are typical of large band gap materials, insulators, with S values typically on the order of 1 V/K. Seebeck

coefficients typically decrease as the carrier concentration increases. Thus semiconductors tend to have *S* values on the order of 100 μV/K and metals typically have *S* values of 1 - 10 μV/K. Conductivity in semiconductors, however, tends to increase as carrier concentration increases. Therefore, in attempting to achieve a high *ZT*, high *S* values in insulators are negated by extremely poor electrical conductivity, and the excellent electrical conductivity of metals is negated by the very low Seebeck coefficient. Thus the electrical conductivity and Seebeck coefficient typically exhibit opposite dependencies on the carrier concentration. Fig 1-3 demonstrates these dependencies and also shows how the power factor, $S^2 s$, varies with carrier concentration. The carrier concentration also has a direct effect on the electronic component of the thermal conductivity, k_e. In the Wiedemann-Franz approximation [2]

$$k_e = L_0 T s \quad , \qquad (3)$$

where L_0 is the Lorentz number equal to about 2.45 X 10^{-8} W-Ω-K^{-2} at room temperature. *T* and s relate the electronic part of the thermal conductivity to the electrical conductivity. Thus tailoring a material through doping to the desired carrier concentration has a large effect on the figure of merit.

In addition to the direct effects of the carrier concentration, the bonding and crystal structure play an important role in creating effective thermoelectric materials. While these properties affect *S*, s, and k_e by altering the band structure, they also strongly affect k_L. By varying the elemental composition to form a variety of different compounds, one may alter all these interrelated properties. While there are literally

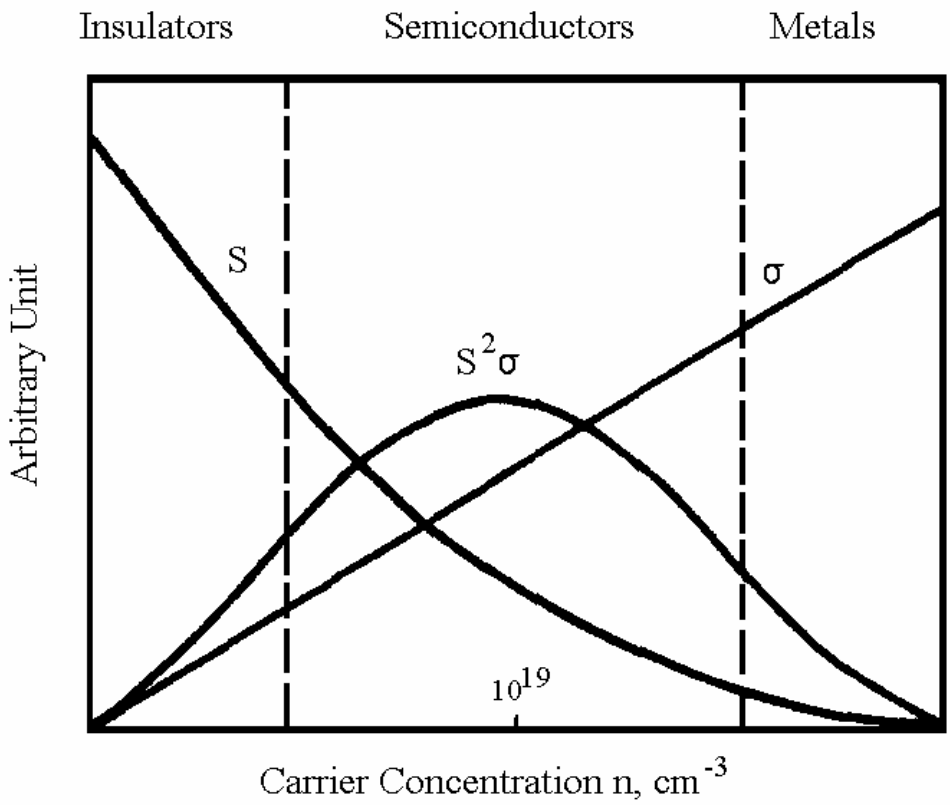

Figure 1-3. **Dependence of *S* and *s* on Carrier Concentration.** Values of the Seebeck coefficient (*S*), electrical conductivity (s), and power factor ($S^2 s$) vs. carrier concentration.

thousands of possible compounds to create, the predicted best combination of these properties direct the search to the semiconductor region since maximal power factors in semiconductors can generally be found in the range where the carrier concentration is approximately 10^{19} cm^{-3} (Figure 1-3) [4].

1.3 Introduction to Thermoelectric Devices

The two principle uses for thermoelectrics are refrigeration and power generation. These applications are illustrated in Figure 1-4 which shows a diagram of a simplified

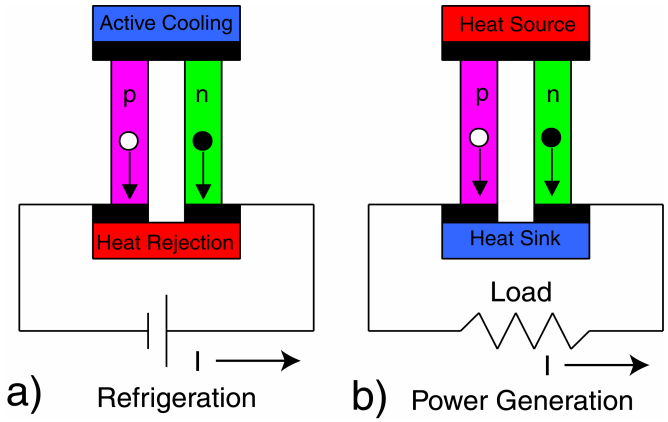

Figure 1-4. **Thermoelectric Effect Illustrated.** The thermoelectric effect illustrated for (a) cooling and (b) power generation applications. The current direction, *I*, is shown in both cases.

thermoelectric module composed of an *n*-type and a *p*-type leg connected through metallic electrical contact pads (black bars).

In order for this effect to be useful, a large enough current must be allowed to pass through the junction at the required voltage. Ideally no heat would be transferred in this process. However, to generate a current, the electrons must be driven from the hot to the cold, taking heat with them. A balance between this heat loss and power conversion must be made. Any heat that travels through other means, such as through thermal conduction, is wasted energy. A final effect that lowers efficiency is the Ohmic resistance. Thus the larger conductivities result in smaller resistive losses.

Applications for thermoelectric refrigeration include cooling of infrared detectors, low noise amplifiers and computer chips where localized cooling and temperature stability is essential. This stability is due to the fact that thermoelectrics are solid-state devices. On the other hand, power generation requires a heat source. The temperature difference between the heat source and the heat sink generates a voltage across the

device. This voltage causes an electric current through the *n*- and *p*-type legs, resulting in power generation across the load for thermoelectric power conversion. Better thermoelectric materials result in larger voltages, and more current consequently producing more efficient devices.

Thermoelectric power generation is currently the main source of energy in deep space spacecraft. The heat source is plutonium, and the heat sink is provided by the cold vacuum of space.(Figure 1-5) This source can last for a very long time as shown by the Voyager probes. A potentially beneficial future use for this type of power conversion is in the automobile industry. By utilizing waste exhaust heat from combustion engines, energy can be harnessed in order to run a vehicle's electrical systems. In general, the advantages of all these solid-state thermoelectric devices are compactness, quietness (no moving parts) and long term reliability.

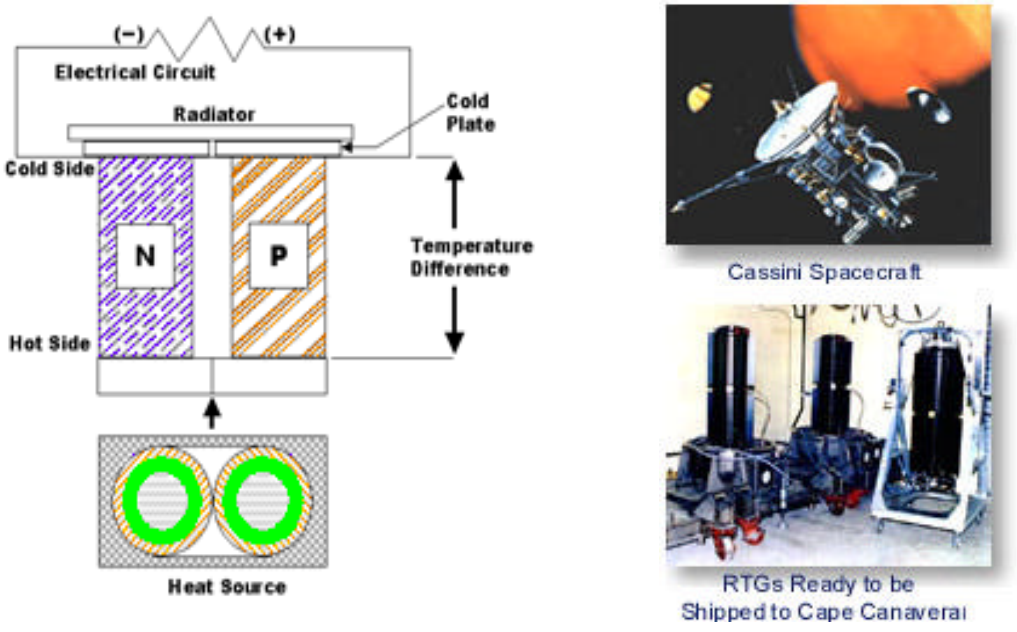

Figure1-5. **Images of Power Generation.** The diagram shows how a plutonium heat source is used to generate electricity. The RTGs are Radioactive Thermoelectric Generators are about four feet tall and used in spacecraft such as Cassini.

Chapter Two: Skutterudites

2.1 Introduction to Skutterudites

Skutterudite refers to a class of compounds with a specific crystal structure. $CoAs_3$ is a mineral that was the first discovered in Skutterud, Norway, giving Skutterudites their name. Materials with this basic structure can be synthesized from many different combinations of elements. These variations result in a large number of possible stoichiometries and thus a wide range of physical properties. These compounds can also be synthesized to possess semiconducting properties. Another primary feature of the Skutterudite crystal structure is the presence of interstitial sites, or "voids", which can be "filled" with a variety of atoms. It is also relatively straightforward to synthesize many of the compounds using standard synthesis techniques. Materials with the Skutterudite crystal structure have shown good potential for thermoelectric applications. Over the last 10 years, research has resulted in steady progress, recently achieving a ZT>1 in Yb [5] and Eu [6] filled Skutterudites. It is hoped that further research will result in greater improvements for thermoelectric power generation applications.

2.2 Skutterudite Crystal Structure

The Skutterudite crystal structure is body centered cubic and has 32 atoms per cubic unit cell. It can be thought of as 8 octants with metal atoms, cobalt for instance, on

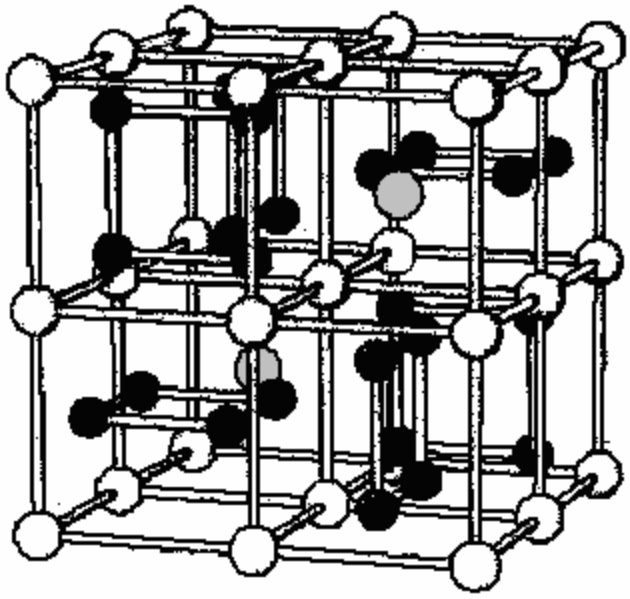

Figure 2-1. **Cubic View of Skutterudite.** The white atoms represent the metal sites such as Co and the black atoms represent the pnicogen sites such as Sb. The large gray atoms in the front top right and back bottom left represent the filler atoms such as Ce.

the corner of each sub-cube, the *c* crystallographic site of its space group, *Im*3. Inside six of these octants are the centers of rings of four pnicogen atoms, such as Arsenic, on the *g* crystallographic site. The other two octants are "empty". (Figure 2-1) The atoms are covalently bonded which produces a semiconducting behavior as well as contributes to its good thermal and electrical properties.

The most basic formula for the unit cell is $X_2M_8Y_{24}$ where X represents the voids in the structure, two per cubic unit cell. These voids can be left vacant, partially filled or completely filled with a variety of elements including group 1 and 2 elements, such as Na or Sr, or one of the Lanthanides, Ce or Eu for example. M represents metal ions, most commonly transition metals such as Cobalt, Rhenium, or Iridium. Y represents pnicogens from group V elements where Phosphorus, Arsenic, or Antimony are the most

common. The bonding (detailed later) in this structure leads to its semiconducting behavior. In a binary Skutterudite, such as $CoSb_3$, there must be 192 valence electrons per cubic unit cell. The addition of dopants leads to a change in this number and the creation of either free electrons or holes. Typically, doping is accomplished on the M sites by using other transition metals such as Fe and Ni. On the Y sites, doping usually employs elements from group IV and VI such as Ge, Se, or Sn.

The bonding of this structure provides many of its interesting features. Each Y atom has four nearest neighbors, two metal atoms and two nonmetal atoms situated at the corners of a distorted tetrahedron. Both the M-Y bond distances and the Y-Y bond distances are short and nearly equal to the sum of the covalent radii, indicating strong covalent bonding. The Y-Y bonding is essential to the stability of the Skutterudite structure and has a large influence on the physical properties. The M-M distances, on the other hand, are quite large, indicating that little bonding occurs between these atoms. The Y-M bonds form a six-fold coordinated irregular octahedron centered on the M atom. The interstitial ion, X, is twelve-fold coordinated by the Y-atom planar groups and is thereby enclosed in an irregular icosahedral "cage" of Y atoms [7]. Figure 2-2 illustrates a complete unit cell for a filled Skutterudite centered at the position of one of the interstitial X or "guest" ions. Large X-ray thermal parameters have been reported for these ions, indicating that they may "rattle" or participate in soft phonon modes in the voids of this crystal structure. Indeed, the thermal parameters of these ions increase with decreasing ionic size. As first pointed out by Slack [3, 8] these ions are "caged" in the

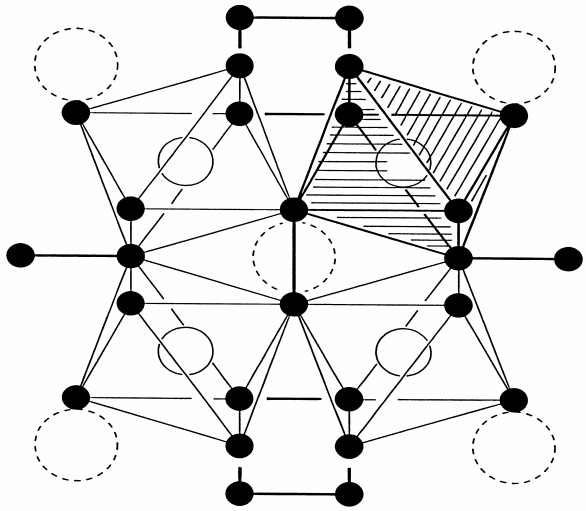

Figure 2-2. **Realistic View of Skutterudite Unit Cell.** The Skutterudite unit cell centered at the void-filler atom (dashed lines), which is enclosed in an irregular icosahedral (12 fold coordinated) cage of pnicogen atoms (black circles). The white circles represent metal atoms. The bonding, however, is inaccurate.

voids of this structure and, if smaller than the void in which they are caged, may "rattle". This localized dynamic disorder interacts in a random manner with the lattice phonons resulting in substantial phonon scattering, particularly the lower wavelength heat carrying modes.

In terms of the electronic bonding, the Y and M atoms are covalently bonded as stated earlier. Each of the Y atoms contributes five electrons to the bonding. Two of these electrons form the two σ bonds to the nearest Y atoms. The other three electrons form the two bonds with the M atoms. The M atoms contribute 9 electrons to the bonding. Three of these form the d^2sp^3 hybrid orbitals in the M-Y bonds and the other six go to the low-spin d^6 state generating diamagnetic behavior.

In the case of filled Skutterudites, nearly all the filler elements have positive valences (typically +2 or +3 for the lanthanides) thus contributing extra electrons to the

192 electrons already present in the unit cell, leading to metallic behavior. For high levels of filling these ions and extra electrons also distort the band structure. To limit the metallic behavior and the band structure distortion, the filler elements must usually be charge compensated through the doping of the M and Y sites. In fact, in order to obtain nearly 100% filling, dopants are required. An additional form of doping comes from lattice vacancies. For example, $CoSb_3$ is always generated *p*-type due to the presence of cobalt vacancies. Vacancies can be formed on the M or Y sites depending on the particular compositions. Much of the research focus on these materials has been on the binary Skutterudites such as $CoSb_3$. As can be seen in Table 1, substantial doping studies on $CoSb_3$ have been performed. All these compounds have been studied to help understand the physics of this interesting material. The general trends show that with increased doping levels, the resistivity decreases, the carrier concentration increases, the Seebeck magnitude decreases, and there is a decrease in the thermal conductivity. The impact of these trends is better described in the next section. Much work has also been performed on filled Skutterudites, with the current best, $Yb_{.19}Co_4Sb_{12}$, showing the largest ZT for *n*-type compounds [5]. However, work on both filled and unfilled binary Skutterudites may have reached the limits of variations that can be synthesized. Perhaps an understanding of ternary Skutterudites such as $CoGe_{1.5}Se_{1.5}$ would provide new avenues of research.

Compound	Nominal x	Actual x	ρ	n	S	κ	Ref.
	×1000	×1000	mΩ-cm	10^{19} cm^{-3}	μV/K	W/mK	
$Ni_xCo_{(1-x)}Sb_3$	1		36.00	0.35	-580	0.87	9,10
300K	5		18.00	1.20	-390	0.74	9,10
	10		10.00	3.30	-320	0.83	9,10
$Fe_xCo_{(1-x)}Sb_3$	5		0.50	2.20	60	1.3	11
300K	20		0.40	5.80	48	0.91	11
	100		1.35	9.20	45	0.30	11
$Cr_xCo_{(1-x)}Sb_3$	10	0.8	10.00	.17			12
300K	20	3.0	8.00	.22			12
	50	8.1	5.00	.09			12
$Fe_xCo_{(1-x)}Sb_3$	10		1.40		120	0.45	13
400K	120		0.80		65	0.37	13
	400		0.95		70	0.25	13
$Pt_xCo_{(1-x)}Sb_3$	30	10	1.27	9.00	-160	0.70	13
300K	50	10	0.83	7.00	-175	0.60	13
	100	40	0.56	15.00	-145	0.50	13
$Pd_xCo_{(1-x)}Sb_3$	10	10	2.86	3.00	-240	0.85	13
300K	50	25	1.81	9.00	-220	0.45	13
	200	50	1.25	20.00	-165	0.30	13
$(Pt+Pd)_xCo_{(1-x)}Sb_3$	60	40	0.67	15.00	-150	0.40	14
	100	65	0.50	40.00	-125	0.26	14
$CoSb_{(3-x)}Te_x$	3		12.5		-400	0.9	15
	30		1.25		-275	0.8	15
	300		0.66		-125	0.5	15

Table 1. Comparison of Doping in CoSb3. Here, r is the resistivity, n is the carrier concentration, S is the Seebeck coefficient and κ is the thermal conductivity.

2.3 Skutterudite Electrical and Thermal Properties

The electronic transport properties of binary Skutterudites were first studied in the late 1950's and early 1960's, and centered on the properties of $CoSb_3$ [2, 16]. From temperature dependent electrical conductivity measurements an energy gap of 0.5 eV was determined. This result is similar to the indirect gap estimated some forty years later by band structure calculations [17]. These theoretical predictions also indicate that the undoped specimens should have low carrier concentrations on the order of insulators.

However for binary compounds, the lowest carrier concentration obtained is about 10^{17} cm^{-3} [16]. In addition, these binary compounds are almost always *p*-type. Doping of these materials can bring them all the way into the metallic regime with carrier concentrations $>10^{21}$ cm^{-3}. It is therefore straightforward to obtain the optimum carrier concentration for thermoelectric applications. Table 1 demonstrates differences in carrier concentration of greater than 2 orders in magnitude, with values ranging from $10^{18}cm^{-3}$ to $4\times10^{20}cm^{-3}$. Thus these materials can be tailored to the desired carrier concentrations once a good base compound has been determined. Table 1 only shows compounds based on $CoSb_3$, but many other binary compounds have been studied as well.

When it was shown that these compounds could support high hole mobilities, it sparked the close scrutiny of the electronic properties of binary Skutterudites as potential thermoelectric materials. For example, Caillat *et al*. [18] reported single crystals of $RhSb_3$ with hole mobility as high as 10^4 cm^2 V^{-1} s^{-1} and $CoSb_3$ with mobilities approaching 2×10^3 cm^2 V^{-1} s^{-1}. Both compounds were shown to possess large Seebeck coefficients consistent with their semiconducting behavior. For the *p*-type semiconductors these mobilities are comparable to that of GaAs and demonstrate the early interest in these semiconductors. (Table 1)

Related to the Hall mobilities, *n*-type Skutterudites have relatively large Seebeck coefficients and effective masses whereas *p*-type compounds have small Seebeck values and effective masses. As seen in the Table 1, *S* values from tens to hundreds of μV/K are often obtained. Also, small changes in composition or dopant can result in positive or negative values for *S*. For instance, doping with less than 0.01 percent nickel results

in the conversion from *p*-type to *n*-type behavior. Adding 0.05 percent Fe makes for strongly *p*-type behavior with an *S* value of 60 μV/K. This sensitivity to dopant is clear from Table 1 with doping changes resulting in Seebeck coefficients from -125 μV/K to 45 μV/K.

In most of the compounds in Table 1, as the carrier concentration increases, the resistivity decreases. Thus the *p*- and *n*-type doping tend to add carriers to the structure and lower the resistivity. However, this results in lower mobilities due to impurity scattering. In spite of this lower mobility, the increased carrier concentration results in lower *S* values. One exception to this trend is Fe. Increased levels of Fe show an *increase* in resistivity with carrier concentration. This demonstrates lower mobility leading to higher resistivity.

The thermal properties of Skutterudites are integral to their potential as thermoelectric materials. Perhaps the two most important mechanisms for conducting heat are conductivity through the lattice and Wiedemann-Franz conductivity due to charge carriers. In semiconductors, it is the first of these properties that conducts most of the thermal energy. Various factors can contribute to this process. For example, grain boundary scattering and lattice defects play an important role. However the most significant change in k_L in Skutterudites comes from the addition of the filler elements. This can alter the lattice thermal conductivity by more than an order of magnitude, as shown in Figure 2-3. The sizes of the "voids" and filler atoms create different ranges and amounts of scattering. Thus the larger elements such as Iridium and Antimony create a

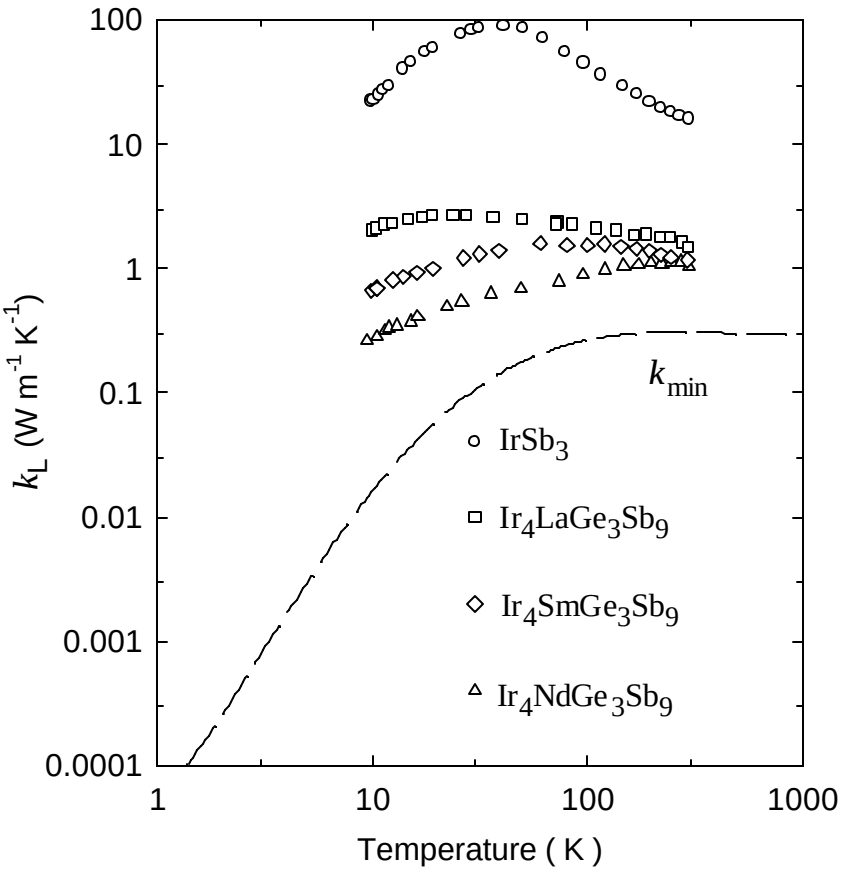

Figure 2-3. Thermal Conductivity of Filled Skutterudites. The decrease in thermal conductivity is clearly shown as the smaller heavier atoms are placed in the voids. Ge is used for charge compensation. k_{min} is the conductivity of an idealized Skutterudite with maximal phonon scattering [19].

larger crystal structure and thus larger voids. The smallest unit cell is 7.7Å, found in CoP_3, and the largest is 9.25Å in $IrSb_3$ [19].

Thus compounds with the Skutterudite crystal structure are of scientific interest due to their unique physical properties. They continue to be of technological interest as well, in particular as potential thermoelectric materials [2]. One important feature of these materials is the large number of different isostructural compositions that can be synthesized. The physical properties of these materials depend sensitively on their

compositions. In particular, the band structure, and thus transport, is dependent on the bonding of the pnicogen site [17]. Thus changes on the pnicogen site can result in a completely new transport in these materials. The diversity of potential compositional variants remains one of the largest reasons why this material system continues to be of scientific and technological interest, and continues to be investigated by many research groups.

Chapter Three: $CoGe_{1.5}Se_{1.5}$

3.1 Introduction to $CoGe_{1.5}Se_{1.5}$

As outlined in the previous chapter, a great deal of research has focused on binary Skutterudites, and $CoSb_3$ in particular. Doping has primarily been performed on the metal site. The primary purpose of that research was to understand how the electronic band structure is changed due to doping. Having reached a basic understanding of how doping affects Skutterudites, it was decided that perhaps a full change in the foundation materials would generate different transport properties. At the least these experiments would provide more information on the Skutterudite's band structure, leading to a further understanding of the physics of these materials, and perhaps also lead to an enhancement of their thermoelectric properties. To this end, Ge and Se can replace Sb completely to generate a different Skutterudite material, $CoGe_{1.5}Se_{1.5}$. Much as GaAs has vastly different properties than pure Si, this new material demonstrates different transport properties as compared to $CoSb_3$.

In addition to the wide range of binary compounds, ternary Skutterudite compounds with simultaneous substitution of group IV and group VI atoms on the pnicogen sites have been previously reported [20, 21]. These compounds should be semiconductors, as they are isoelectronic with $CoSb_3$. Ternary Skutterudites have been synthesized previously through various methods and some basic information about them was

gathered. The earliest work was done by Korenstein *et al*. [20] on $CoGe_{1.5}S_{1.5}$ and $CoGe_{1.5}Se_{1.5}$ synthesized with the chemical vapor transport method using iodine as the transport agent. Structural and magnetic measurements were then performed on the samples. The X-ray data indicated that the structure was nearly identical to that of $CoAs_3$, with a probable short range ordering in $CoGe_{1.5}S_{1.5}$ with rhombohedral symmetry. $CoGe_{1.5}S_{1.5}$ had a lattice parameter of 8.017 Å, a density of 5.54 g/cm^3, was diamagnetic, and found to decompose at 1000 °C. $CoGe_{1.5}Se_{1.5}$ had a lattice parameter of 8.299 Å, a density of 6.62g/cm^3, was diamagnetic, and decomposed at 800 °C.

This precipitated attempts by Lyons *et al*. [21] to synthesize Ir and Rh containing compounds of similar compositions. Many samples were attempted using direct combination of the elements such as $IrSn_{1.5}Se_{1.5}$, $IrSi_{1.5}S_{1.5}$, $IrSi_{1.5}Se_{1.5}$, $RhSn_{1.5}S_{1.5}$, $RhGe_{1.5}Se_{1.5}$, and $RhSn_{1.5}Se_{1.5}$. In addition, the vapor deposition technique was attempted for both $RhSn_{1.5}S_{1.5}$ and $RhSn_{1.5}Se_{1.5}$. All of these specimens failed to produce pure samples; however four single phase samples were synthesized: $IrGe_{1.5}S_{1.5}$ with a lattice parameter of 8.2970Å, $IrGe_{1.5}Se_{1.5}$ at 8.5591 Å, $IrSn_{1.5}S_{1.5}$ at 8.7059Å, and $RhGe_{1.5}S_{1.5}$ with a lattice parameter of 8.2746Å. In addition, the X-ray spectra showed some of the same ordering as seen by Korenstein *et al*. [20]. All of these samples demonstrated diamagnetic behavior. Sintered bars were made for $IrGe_{1.5}S_{1.5}$ and $IrGe_{1.5}Se_{1.5}$ for resistivity measurements. Room temperature values were 20 Ω-cm for the Sulfide and 4 Ω-cm for the Selenide. The data was taken over a range of a few hundred degrees and indicated activation energies of 0.11 and 0.076 eV respectively.

The success of synthesizing ternary Skutterudites, and the lack of information on the transport properties led to our further studies on these mixed-anion materials. Two specimens of $CoGe_{1.5}Se_{1.5}$ were made, one *p*-type and one *n*-type. As will be discussed below, the basic measurements of crystal structure and density along with transport measurements were performed.

3.2 Specimen Preparation

Typical specimen preparation began with the mixing of elements from 99.99% pure 22 mesh cobalt powder from Alfa Aesar, intrinsic germanium ground to 325 mesh in a Nitrogen atmosphere glove box, 99.999% pure selenium shot from Asarco. The elements were weighed to within 0.2 mg of the stoichiometric target weights. First, the stoichiometry was used to roughly calculate the masses of each element needed to produce approximately 4 grams of each compound. Then selenium shot was measured and weighed to be within a few tenths of milligrams of the desired amount calculated above. The precise amount of selenium was then used to calculate the exact amounts needed to get the desired stoichiometry. The initial specimen of $Co_4Ge_6Se_6$ (S002) used the desired stoichiometry as the starting stoichiometry. It was found that selenium condensed outside of the specimen during heating, thus all later specimens (including S008) started with 9% extra selenium, for example $Co_4Ge_6Se_{6.5}$ to result in a $Co_4Ge_6Se_6$ composition. This value was calculated by determining the total loss during the synthesis process.

Having determined the stoichiometry, cobalt and germanium were weighed and mixed for 2 minutes. The resulting powders were placed with the selenium shot in a Pyrolite boron nitride (BN) crucible and mixed again. The BN crucible was then placed at the bottom of a quartz ampoule with a disk of Grafoil™ placed over the crucible. A small piece of quartz tube was fitted inside the ampoule in preparation to make an air tight seal.

Once the setup was completed, a custom vacuum purging system was used to purge oxygen out of the tube and replace it with nitrogen. The purging system used a Welch Duoseal 1405 vacuum pump. This was attached to a system of valves along with a line to the ultra high purity (99.999%) nitrogen tank and a pressure gauge. To connect the valve system to the quartz, reinforced rubber hose was connected to large diameter vacuum hose. A seal was made between this large vacuum hose and the quartz through rugged hose clamps, allowing for $<10^{-2}$ Torr of pressure in the tube. Once a good seal was made, the tube was pumped for approximately 5 minutes and back filled with nitrogen. This procedure was repeated twice more, and left at slightly below one atmospheric pressure to aid in sealing. A hydrogen-oxygen torch was used to fuse the small inner piece of quartz to the tube. This procedure ensured that the specimen inside the BN crucible was in an inert environment.

The sealed quartz ampoule was then placed inside a Mellen TC12 tube furnace oriented vertically. The furnaces were set to achieve a zone of 700 degrees Celsius where the temperature did not vary more than 2 degrees over the length of the ampoules. The specimens were left inside the furnace for four days after which time they were air

quenched. They were then visually inspected to check for Se condensation on the quartz. Once they were cooled to room temperature, the specimens were removed. The extra selenium was gathered and weighed separately to estimate the Se loss in each Specimen. The material was then evaluated for appearance and weighed.

After the specimens were weighed, they were ground to a fine powder inside a nitrogen atmosphere glove box. The finely ground powder was then placed in a high strength steel die and cold pressed to 64,000 PSI using a Carver Laboratory Press to produce a pellet. The pellet was weighed and placed into a BN crucible, sealed in quartz with a similar procedure as described above, and put into the furnace at 700 degrees. It was heated for four days and then air quenched. This process of grinding and heating was performed for a total of three times, to produce a single phase specimen.

For X-ray diffraction measurements (XRD) a small amount of powder for each specimen was mixed with a small amount of a silicon standard (NIST 640c) and placed on a glass slide. A Rigaku Miniflex X-ray Diffractometer was used. Typically the diffraction spectra were taken between 20 and 80 degrees 2Θ. An identification program (Jade™) in conjunction with Excel™ spreadsheet software was used to determine their lattice parameters and if any impurities were present.

The powdered specimen was then hot pressed (Thermal Technologies HP20-4560-20) in a graphite die with a 0.5-inch diameter. After being preloaded to 1,500 PSI, it was heated to 650 °C while under 25,000 PSI of pressure in a nitrogen atmosphere for 2 hours. Grafoil™ was used to separate the specimen from the molybdenum punches that applied the pressure.

After hot pressing, the Grafoil™ was removed from the specimen, and a wire saw used to cut the specimen to minimize surface damage. Boron carbide suspended in a mixture of water and glycerin was used as the cutting fluid. A small piece was also cut and mounted in a one inch epoxy puck for metallographic analysis. The specimen in the puck was then polished in steps down to a final polishing round of 0.3 micron alumina. A solution of aqua regia was used to etch the specimen and allow the grain structure to become clearly visible. A Unimet light microscope was used in conjunction with a Panasonic CCD camera to photograph the grain's surface for analysis and grain size measurements. The line-boundary method (ASM Standard) was used to determine the grain sizes.

In addition to visual analysis, four probe resistivity and Seebeck measurements were performed at room temperature on specimens cut to $2\times2\times5$ mm^3. To determine the Seebeck coefficient, a custom made setup was used consisting of two copper disks 1 inch in diameter. One disk was attached to a large aluminum heat sink through a non-electrically conducting, good thermally conducting glue. The other was mounted on a spring-loaded press. A heater coil was located inside the upper disk and attached to a voltage source to raise the temperature. Two small holes were drilled into the sides of the disks for thermocouples. A multimeter was used to determine the voltage generated as the temperature was varied. These room temperature measurements were in agreement with those described in section 3.4 below.

3.3 Crystal Structure

Two particular $CoGe_{1.5}Se_{1.5}$ specimens, labeled S002 and S008, will be described herein. Each demonstrates the Skutterudite crystal structure with the Ge and Se on the pnicogen sites and Co on the metal site. No clear ordering on the pnicogen site of Ge and Se has been determined from our XRD analysis; however previous studies of this composition indicated short range rhombohedral ordering. X-ray diffraction patterns and electron probe microanalysis (EPMA) were used to determine the structure and composition of these compounds. Optical microscopy was used to evaluate the grain size of each specimen.

The specimen S002 was made with a starting stoichiometry of $CoGe_{1.5}Se_{1.5}$, exactly that for the Skutterudite structure with the same amounts of Ge and Se. The resultant stoichiometry was determined to be $CoGe_{1.452}Se_{1.379}$ from electron-beam microprobe analysis (EMPA) with the Ge and Se concentrations assigned relative to full occupation of Co on the metal crystallographic site. This compound is an *n*-type semiconductor. The evaporation and re-condensation of Se from the specimen due to a possible 1-degree temperature gradient in the range of the sample space of the furnace combined with the high vapor pressure of Se may have resulted in the low levels of Se. The second specimen (S008) was synthesized with 9% extra Se to counter this loss, or by starting with $CoGe_{1.5}Se_{1.625,}$ and resulted in a final stoichiometry of $CoGe_{1.431}Se_{1.385}$. This specimen is a *p*-type semiconductor. These specimens, along with others synthesized, demonstrated a tendency towards a general stoichiometry of $CoGe_{1.45}Se_{1.38}$.

From the XRD data both S002 and S008 have the same lattice parameters to within experimental uncertainty. The two specimens were single phase in both the XRD and the EMPA analyses. Optical micrographs demonstrated pure phases, and were also used to estimate the sizes of these polycrystalline specimens. The room temperature physical parameters of the specimens are summarized in Table 2. The theoretical density for $CoGe_{1.5}Se_{1.5}$ is 6.65g/cm^3. The expected densities calculated from the EPMA analysis show that S002 should be 6.35g/cm^3, and S008 should be 6.32 g/cm^3. The measured densities show that the specimens were hot pressed to 88 and 92 percent respectively of their theoretical densities. As seen in Table 2, the specimens' lattice parameters and grain sizes are similar, while their electrical properties are very different. Room temperature values for these properties were obtained as described in the section on specimen preparation. The specimens were sent to Dr. Jihui Yang of General Motors R&D for temperature dependent electrical, thermal and magnetic measurements. The room temperature measurements agree with those of General Motors. Transport properties were then modeled to understand the physics of these compounds.

Specimen	a	Grain Size	d	S	ρ
S002	8.306±0.008	4.6	5.61	-550	1.2
S008	8.296±.0004	3.9	5.82	350	2.5

Table 2. **Data on $CoGe_{1.5}Se_{1.5}$.** Here, a is the lattice parameter in Å, d is the density in g/cm^3, S is the Seebeck Coefficeint in μV/K, and r is the resistivity in Ω-cm. All data are at room temperature.

3.4 Electrical Properties

Figure 3-1 shows the resistivity vs. temperature data for S002 ($CoGe_{1.452}Se_{1.379}$) and S008 ($CoGe_{1.431}Se_{1.385}$). For comparison $CoSb_3$ is also shown in the figure. From Figure 1, r decreases with increasing temperature, showing typical semiconducting behavior for both specimens. Over the entire temperature range the $CoGe_{1.5}Se_{1.5}$ specimens have higher r values than $CoSb_3$ with S002 showing the larger resistivity.

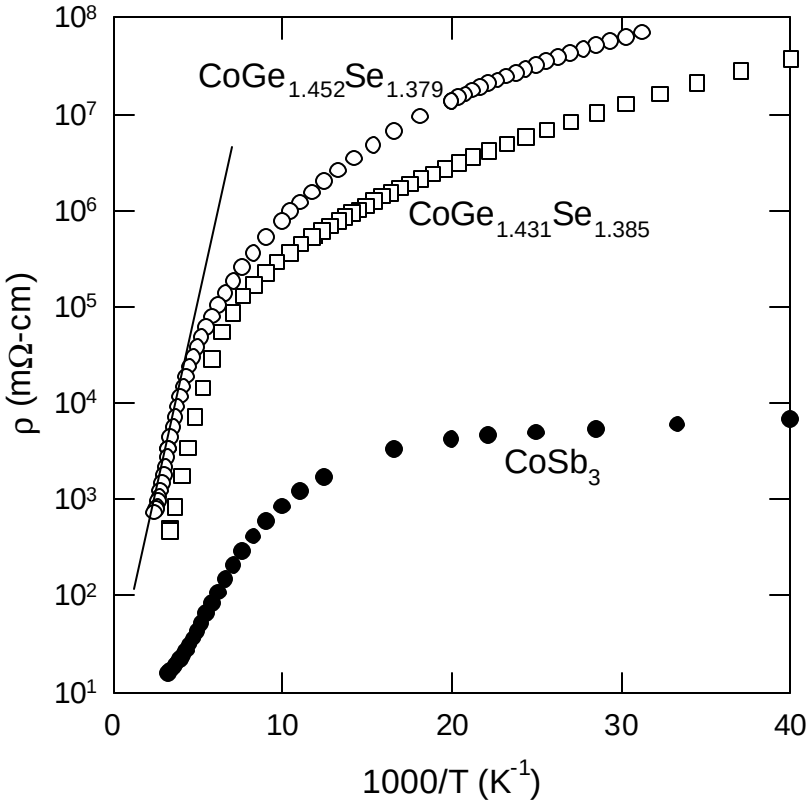

Figure 3-1. **The Electrical Resistivity of $CoGe_{1.5}Se_{1.5}$ and $CoSb_3$ versus Temperature.** $CoGe_{1.452}Se_{1.379}$ is S002 and $CoGe1_{.431}Se_{1.385}$ is S008. The solid line is a fit of the form $r = r_0\exp[E_a/k_BT]$ to the higher temperature data, indicating E_a = 0.168 eV.

The straight line is a fit to the high temperature data (T > 300 K) using $r = r_0 \exp[E_a/k_B T]$, where E_a is the activation energy. The fit results give E_a = 0.168 eV and could imply an intrinsic semiconducting band gap of ~ 0.336 eV. A fit for S008 yields the same activation energy. This estimated intrinsic band gap, higher than a gap of 0.102 eV for $CoSb_3$ [9]. Similar estimates on $IrGe_{1.5}S_{1.5}$ and $IrGe_{1.5}Se_{1.5}$ indicated an activation energy of ~ 0.1 eV; however, the authors in Ref. 20 suggested that the intrinsic gap may be even higher. We know of no band structure calculations for this material. At room temperature, $r = 3.37\times10^3$ and 4.703×10^2 mΩ-cm for S002 and S008 respectively. The difference increases with decreasing temperature. We speculate that the difference in r between specimens S002 and S008 is due to the different amounts of vacancies on the g crystallographic site.

As shown in Figure 3-2, the negative and positive S values indicate that electrons and holes are the majority carriers for S002 and S008 respectively. At room temperature a large value of - 550 μVK^{-1} for S is observed for S002 decreasing to + 350 μVK^{-1} for S008. The upward trend for the higher temperature data for S002 is likely due to the increase in p-type conduction for higher temperatures. Consistent with the S data, our Hall measurements also show that the carriers are electrons for S002. The inset shows the electron concentrations obtained from the Hall measurements. At room temperature $n \sim 3.5\times10^{18}$ cm^{-3}. We believe prolonged hot-pressing could cause lattice vacancies on the Ge or Se sites in $CoGe_{1.5}Se_{1.5}$, resulting in n-type electrical conduction for S002 [22, 23]. The sintered or quickly hot-pressed undoped $CoSb_3$ specimens are usually p-type semiconductors due to excess Sb, or deficient Co, in the crystal lattice [24, 25].

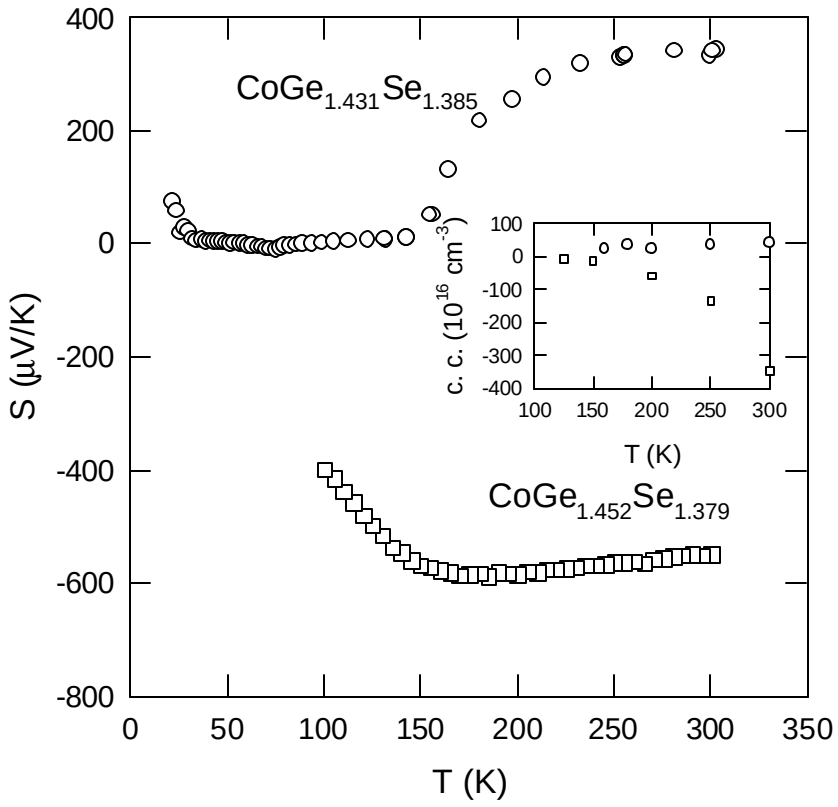

Figure 3-2. **Seebeck Coefficient Versus Temperature of $CoGe_{1.5}Se_{1.5}$.** Both *n*-type S002 and *p*-type S008 are shown. The inset shows carrier concentration from Hall measurements for the two specimens.

S008 is believed to have resulted in *p*-type electrical conduction due to the slight change in stoichiometries. This demonstrates the flexibility to control the properties of these materials through very precise balancing of the stoichiometry, illustrated best by the dramatic change in *S* values from negative to positive for the small change in the Ge to Se ratio. The electron mobility varies roughly as $T^{0.66}$ near room temperature with values of 0.53 to 0.26 $cm^2V^{-1}s^{-1}$ from room temperature to 125 K. This indicates mixed ionized impurity and acoustic lattice scattering of electrons.

For a single parabolic band S and n are given by [26]

$$S = \pm \frac{k_B}{e}\left(\frac{(2+r)F_{1+r}(h)}{(1+r)F_r(h)} - h\right) \quad , \tag{11}$$

$$n = 4p\left[\frac{m^* k_B T}{h^2}\right]^{3/2} F_{1/2}(h) \quad , \tag{12}$$

where r is the exponent of the energy dependence of the electron mean free path, m^* is the electron effective mass, e is the electron charge, $h = E_F / k_B T$ is the reduced Fermi energy, E_F is the Fermi energy, and F_x is the Fermi integral of order x. The + and – signs in Eq. (11) are appropriate for holes and electrons, respectively. For electrons scattered by ionized impurities and acoustic phonons, r = 2 and 0, respectively. We use the intermediate value r = 1 for mixed scattering [27]. The room temperature S and n data yield $m_e^* = 2.55\, m_o$, where m_o is the electron mass. This value of m_e^* is slightly smaller than that of $CoSb_3$ [9]. The room temperature value of hole mobility for $CoGe_{1.431}Se_{1.385}$ is ~ 35 $cm^2V^{-1}s^{-1}$, and varies approximately as T^6 between 160 K and 300 K. With the limited data points, it is difficult to ascertain the hole scattering mechanism, however assuming r=1, $m_h^* = 0.1\, m_o$. Based on the much higher hole mobility, a small effective mass for holes is reasonable. Similar results were found in $CoSb_3$ [10].

3.5 Thermal Properties

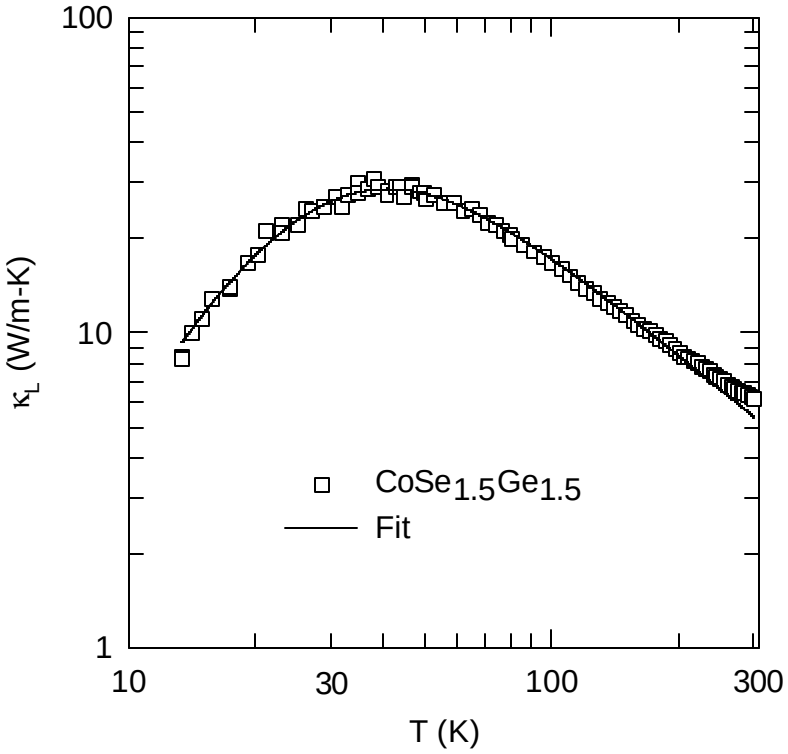

Figure 3-3. **Lattice Thermal Conductivity for $CoGe_{1.5}Se_{1.5}$ (S002) Versus Temperature.** The open squares are the experimental data and the line is a fit based on Eqs. (13) and (14).

Figure 3-3 show the lattice thermal conductivity, k_L, of S002. Typical temperature dependence for crystalline materials is observed with a room temperature value of 6 $Wm^{-1}K^{-1}$. The total thermal conductivity can be written as $k = k_L + k_e$. The electronic thermal conductivity k_e was calculated using the Wiedemann-Franz relation ($k_e = L_0 T/r$ with $L_0 = 2.45\times10^{-8}$ V^2K^{-2}) from the measured r. In this approximation

almost all of the thermal conduction is due to the lattice phonons because at all temperatures k_e is less than 1% of k. The k_L values are lower than those of $CoSb_3$ which have $k_L \sim 8$ $Wm^{-1}K^{-1}$ at room temperature [10, 11, 28]. The solid line in Fig. 3-3 is a theoretical fit of the data using the Debye approximation:[10, 11, 29]

$$k_L = \frac{k_B}{2p^2 u}\left(\frac{k_B T}{\hbar}\right)^3 \int_0^{q_D/T} \frac{x^4 e^x}{t_C^{-1}(e^x - 1)^2} dx \quad , \qquad (13)$$

where $x = \hbar w / k_B T$ is dimensionless, w is the phonon frequency, k_B is the Boltzmann constant, $\hbar$ is the reduced Planck constant, q_D is the Debye temperature, u is the velocity of sound, and t_C is the phonon scattering relaxation time. The phonon scattering relaxation rate t_C^{-1} can be written as:

$$t_C^{-1} = \frac{u}{L} + Aw^4 + Bw^2 T \exp(-\frac{q_D}{3T}) \quad , \qquad (14)$$

where L is the grain size and the coefficients A and B are the fitting parameters. The terms in Eq. (14) represent grain boundary scattering, point defect scattering, and phonon-phonon Umklapp scattering, respectively. In the solid line theoretical fit of Fig. 3-3, L = 1.3 μm, $A = 4.70\times10^{-43}$ s^3, and $B = 6.66\times10^{-18}$ sK^{-1}. The fitting parameters are very close to those of $CoSb_3$, [10, 11] except that A (the pre-factor for point defect

scattering) is approximately 2 times larger. This is reasonable in light of the large number of vacancies on the *g* crystallographic site indicated by EMPA. We expect that alloy scattering between Ge and Se plays a smaller role in the enhanced point defect phonon scattering in this specimen because of the small mass difference (~ 8%) between Ge and Se. The solid line in Fig. 3-4 models the overall temperature dependence of k_L quite well over the entire temperature span.

3.6 Magnetic Properties

In addition to the standard electronic and thermal property measurements, the magnetic moment M was found to vary linearly with the magnetic field H for H < 5 T between 2 K and 300 K. The magnetic susceptibility ($c = \frac{M}{H}$, measured at H = 0.5 T) as a function of temperature for both S002 and S008 is shown in Figure 3-4. Data for polycrystalline $CoSb_3$ from Ref. 9 are also shown for comparison. For T > 100 K, both samples exhibit diamagnetic behavior almost identical to that of $CoSb_3$. This indicates that Co atoms assume the low-spin d^6 electronic configuration, the same as in $CoSb_3$. The much larger Curie-Weiss type component for S002 at T < 100 K is believed to be due to the magnetic impurities (Fe and Ni) in the starting material Co [25, 30].

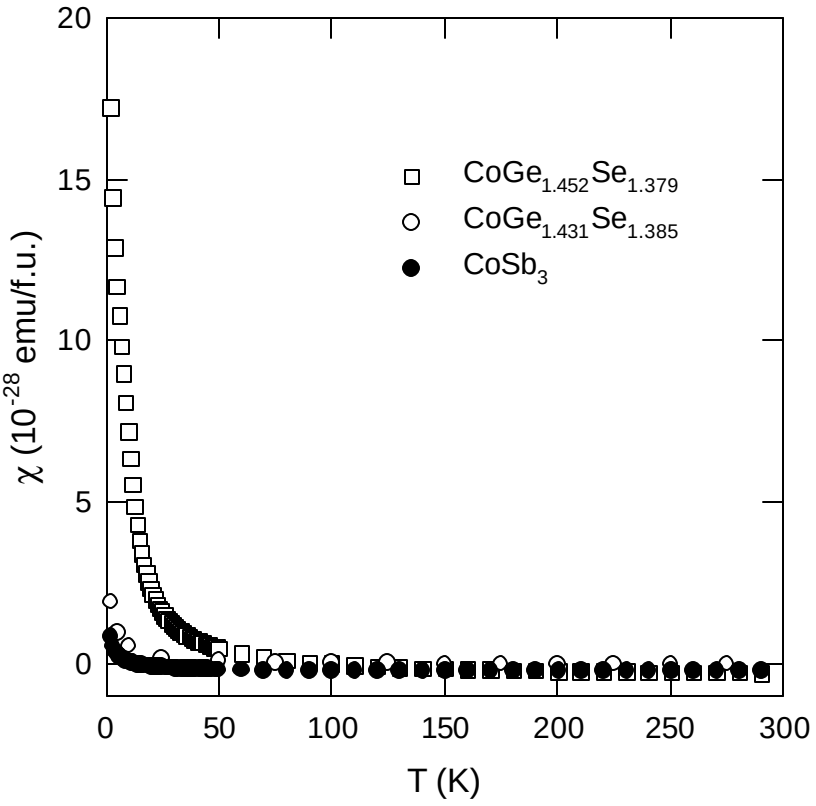

Figure 3-4. **Magnetic Susceptibility of Polycrystalline $CoGe_{1.5}Se_{1.5}$.** Data for polycrystalline $CoSb_3$ are also shown for comparison.

Chapter Four: Summary of Results

Many materials and synthesis techniques are currently being employed in the investigation of new and novel classes of materials for potential applications in technologically important fields. Solid-state thermoelectric power conversion is one field of interest. The investigation of a class of materials known as Skutterudites continues to be of interest for thermoelectric applications. The fact that many different compositions can be synthesized in this crystal structure, together with the ability to 'tune' the transport properties as a function of stoichiometry, encourages researchers to pursue avenues of optimization within this class of materials. The basic understanding of the transport properties of the different compositions is key however and will be the basis for an in depth understanding and evaluation of the thermoelectric properties of these materials towards further optimization and development.

In this report the Skutterudites $CoGe_{1.452}Se_{1.379}$ (S002) and $CoGe_{1.431}Se_{1.385}$ (S008) were synthesized in order to further our basic knowledge and understanding of these interesting materials as well as begin an investigation into their potential for thermoelectrics applications. It was observed that the electrical transport properties are quite different than that of $CoSb_3$. In particular a small compositional difference between the two specimens S002 and S008 had a dramatic effect on the carrier type, carrier concentration and *S* values. This is very interesting in terms of potential for optimization.

as it allows for the "tuning" of the electronic properties. The relatively high room temperature Seebeck coefficients are also promising for thermoelectric applications, although their high resistivity is an obstacle. Research on void filling and doping of these interesting materials is therefore warranted in continuing the research into these Skutterudites.

In summary, the specimens prepared for this report were synthesized by mixing and reacting high purity Co, Ge and Se. These compounds are diamagnetic semiconductors with a relatively large band gap as compared to $CoSb_3$. The electrical and thermal conduction are influenced by the vacancies in the crystal lattice because of the non-stoichiometry of the specimens. The low mobility of $CoGe_{1.452}Se_{1.379}$ and $CoGe_{1.431}Se_{1.385}$ precludes them from being useful thermoelectric materials; however, the large Seebeck coefficients make them interesting for further investigation. The carrier types in these compounds depend sensitively on vacancies as well as the ratio between Ge and Se, offering a method for tuning the electrical transport properties of these compounds. The room temperature thermoelectric figure of merit is ~ 0.0005. Although this value is low this research opened the door to further research into these and similar compositions of Skutterudites and began an in depth understanding of their transport properties. The work reported herein has been accepted for publication in Physical Review B and is scheduled for publication in November 2004.

References

1. W. Thomson, Proc. Roy. Soc. Edinburgh, Trans. **21**, Part I, 123 (1857)
2. G.S. Nolas, J. Sharp, H. J. Goldsmid: *Thermoelectrics: Basic Principles and New Materials Developments* (Springer, New York, 2001)
3. G.A. Slack and V. Tsoukala, J. Appl. Phys. **76**, 1665 (1994).
4. I. B. Cadoff, E. Miller: *Thermoelectric Materials and Devices* (Chapman & Hall, London, 1960)
5. G.S. Nolas, M. Kaeser, R. Littleton, IV and T.M. Tritt, 'High figure of merit partially Ytterbium filled skutterudite materials', Appl. Phys. Lett. **77**, 1822 (2000).
6. G.A. Lamberton, Jr., S. Bhattacharya, R.T. Littleton IV, T.M. Tritt and G.S. Nolas, 'High figure of merit in Eu-filled CoSb3 skutterudites', Appl. Phys. Lett. **80**, 598 (2002).
7. C. Uher, 21st *International Conference on Thermoelectrics,* A2-1 #570 2002
8. G.A. Slack, Symp. Proc. Mater. Res. Soc. **478**, 47 (1997)
9. Jeffery S. Dyck, Wei Chen, Jihui Yang, Gregory P. Meisner, Ctirad Uher, Pysical Review B, **65**, 115204 (2002)
10. J. Yang, D.T. Morelli, G.P. Meisner, W. Chen, J.S. Dyck, C. Uher, Physical Review B, **65**, 094115 (2002)
11. J. Yang, G. P. Meisner, D.T. Morelli, C. Uher, Physical Review B, **63**, 014410 (2000)
12. J. Yang, M.G. Endres, G. P. Meisner, Physical Review B, **66**, 014436 (2002)
13. S. Katsuyama, Y. Sihichijio, M. Ito, K Majima, H. Nagai, Journal of Applied Physics, **84**, No. 12, 6708 (1998)
14. H. Tashiro, Y. Notohara, T. Sakakibara, H. Anno, K. Matsubara, 16th *International Conference on Thermoelectrics*, 326, IEEE, 1997
15. Krzystof T. Wojciechowski, Materials Research Bulletin, **37**, 2023-2033, (2002)
16. J.P.Fleurial, T. Caillat, A. Borshchevsky 16th *International Conference on Thermoelectrics*, 1, IEEE, 1997
17. I. Lefebvre-Devos, M. Lassalle, X. Wallart, J. Olivier-Fourcade, L. Monconduit, J.C. Jumas, Phys. Rev. B, **63**, 125110, (2001)
18. T. Caillat, J.-P. Fleurial, and A.J. Borshchevsky, Cryst.Growth **166**, 722 (1996)
19. G.S. Nolas, G.A. Slack, D. T. Morelli, T. M. Tritt, A.C. Ehrlich, J. Appl. Phys, **79**, 4002 (1996)
20. R. Korenstein, S. Soled, A. Wold, G. Collin, Inorganic Chemistry, **16,** No. 9, 2344 (1977)
21. A. Lyons, R. P. Gruska, C. Case, S. N. Subbarao, A. Wold, Materials Research Buliten, **13,** 125, (1978)
22. L. D. Dudkin and N. Kh. Abrikosov, Sov. Phys. Solid State **1**, 126 (1959)
23. J. W. Sharp, E. C. Jones, R. K. Williams, P. M. Martin, and B. C. Sales, J. Appl. Phys. **78**, 1013 (1995)
24. G.S. Nolas, D.T. Morelli, and T.M. Tritt, Annu. Rev. Mater. Sci. **29**, 89 (1999), and references therein
25. C. Uher, in *Semiconductors and Semimetals*, Vol. **69**, edited by Terry M. Tritt (Academic Press, New York, NY, 2000), pp. 139-254, and references therein
26. V. A. Johnson, *Progress in Semiconductors*, edited by A. F. Gibson (Heywood, London, 1956), Vol. **1**, pp. 65-97
27. G. A. Slack and M. A. Hussain, J. Appl. Phys. **70**, 2694 (1991).
28. J. Callaway, Phys. Rev. **113**, 1046 (1959)
29. G. S. Nolas, J. L. Cohn, and G. A. Slack, Phys. Rev. B **58**, 164 (1998)
30. H. Anno, K. Hatada, H. Shimizu, K. Matsubara, Y. Notohara, T. Sakakibara, H. Tashiro and K. Motoya, J. Appl. Phys. **83**, 5270 (1998)